Strategy and validation of large-scale MRI registration framework

I. Csapo[1], C. M. Holland[1,2], and C. R. Guttmann[1]

[1]Center for Neurological Imaging, Brigham and Women's Hospital, Boston, MA, United States, [2]Department of Anatomy & Neurobiology, Boston University School of Medicine, Boston, MA, United States

Objective: MRI studies are often based on quantitative image analysis that requires the transformation of different images into a common space. This enables, for example, the comparison of the distribution of pathology between groups of subjects or the construction of probabilistic atlases incorporating thousands of images [1]. In the context of large MRI studies, calculating the transforms that relate each image to every other image is possible; however, the number of such transforms makes it prohibitive. We therefore propose an efficient strategy that relies on the computation of a single transform per image relating it to the previous image of the same individual or to an anatomical atlas. Individual transforms could then be mathematically concatenated to relate any pair of images. We show that this approach is valid when relating images from an individual subject acquired at multiple time-points.

Methods: Experiments were performed on a longitudinal dataset of 10 multiple sclerosis patients (37±10.0 years old at the time of the first scan) with 9 serial (6±4.1 months between scans; 4.0±0.98 years between first and last intra-patient time points) dual-spin echo 1.5 T MRI scans (TR 3000 ms, TE 30ms/80ms, field of view 24 cm, acquisition matrix 256x192, 3mm slice thickness). Intra-subject registrations were performed on the PD images and transforms (T) linking multiple time points together were concatenated. The images from time point 9 (I_9) through time point 2 (I_2) were registered to the preceding time points (step-wise consecutive, e.g. T_{54}) using the FMRIB Linear Image Registration Tool (FLIRT, FMRIB Oxford, UK) [2]. For each time point from I_9 to I_3, the step-wise consecutive transformation matrices linking all previous time points to the baseline were concatenated (e.g. T_{9-1}). In addition, I_9 through I_3 were also directly registered to the baseline (e.g. T_{91}), providing the comparison transforms for evaluating the concatenated transforms. For each subject, images for time points I_9 through I_2 and the transformed images were intensity normalized [3] after skull-stripping to the baseline in order to facilitate the registration evaluation with Pearson correlation (r), an intensity-based metric. Registration quality was assessed by calculating the correlation between each image pair within the skull-stripped target image. Automated tissue classification was also performed [4] yielding volumetric information. Brain parenchymal fraction (BPF), the ratio of brain tissue volume normalized to the ICC, was used to assess the extent of tissue loss over time and its impact on the quality of the co-registrations. Student's t-test was used to compare the Pearson correlation coefficients between images resampled with the direct (e.g. I_{T91}) and concatenated transforms (e.g. I_{T9-1}). Changes in BPF over time and changes in WMH volumes were assessed.

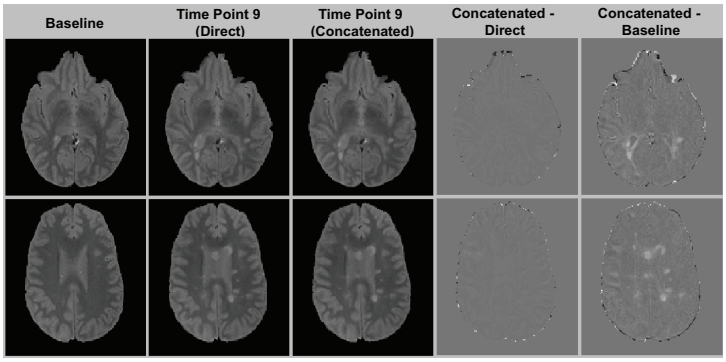

Fig. 1: Visual comparison of concatenated versus direct registration. Columns from left to right: first time point; direct (I_{T91}) registration; concatenated (I_{T9-1}) registration; subtraction image of I_{T9-1} and I_{T91}; subtraction image of I_{T9-1} and I_1. Changes due to atrophy and disease activity are apparent between the baseline and time point 9.

Results: The direct ($r_{91,1}$) and concatenated ($r_{9-1,1}$) correlation coefficients were not significantly different (p=0.84), with a mean correlation coefficient between the I_{T91} and the I_{T9-1} images of 0.99 (±0.012). In Figure 1, we present images from a single subject showing slices from the I_{T91} image, that is a result of registering I_9 to I_1 directly, for comparison with the I_{T9-1} image, that is obtained by applying the T_{9-1} concatenated transform to I_9. The subtraction image of I_{T91} and I_{T9-1} shows minimal difference. The correlation coefficients for individual subjects are presented in Table 1.

Table 1: Correlation coefficient (r) for direct and concatenated registrations of time point 9 to 1.

Subj.	I_{T91} vs. I_1 (Pearson r)	I_{T9-1} vs. I_1 (Pearson r)	I_{T91} vs. I_{T9-1} (Pearson r)
1	0.79	0.80	0.99
2	0.74	0.75	1.00
3	0.69	0.70	0.99
4	0.63	0.63	1.00
5	0.88	0.87	0.99
6	0.69	0.69	0.99
7	0.73	0.73	0.98
8	0.76	0.76	0.99
9	0.74	0.74	0.99
10	0.72	0.71	0.95
Mean	0.74 (± 0.07)	0.74 (± 0.07)	0.99 (± 0.01)

All intra-subject step-wise consecutive registrations were successful, yielding a mean correlation coefficient of 0.81 (± 0.075; range: 0.41-0.90) across the 10 subjects. Time point 3 of subject 10 had a significant signal inhomogeneity artifact that adversely affected the correlation coefficients of the T_{32} and T_{43} step-wise consecutive transformations ($r_{32,2}$: 0.45, $r_{43,3}$: 0.42) and the T_{41} direct transformation ($r_{31,1}$: 0.40). However, registration quality did not appear to be affected as evident from visual inspection and the correlation coefficients of the concatenated transforms that included time point 3 (e.g. $r_{4-1,1}$: 0.74, $r_{5-1,1}$: 0.76).

In order to assess the contribution of potential confounding variables to the registration quality, the correlations between the direct and concatenated correlation coefficients and the following variables were evaluated: absolute change in BPF, absolute change in ICC volume, absolute change in WMH volume, and time elapsed between time points. Differences in BPF showed significant inverse correlation with the correspondence of the resampled images (direct: r= -0.28, p=0.021; concatenated: r= -0.29, p=0.013). The other variables had no significant effect on registration quality.

Discussion: The results illustrate that the images realigned via the direct and indirect methods are essentially equivalent even in the context of atrophic and other disease-related structural changes, demonstrating the validity of the proposed approach. The applicability of this strategy is especially relevant in the context of voxel-based morphometry analyses such as relating lesion distribution patterns to functional deficits (e.g. gait or cognitive performance) or disease biomarkers (e.g. genetic markers or known disease risk factors) [5]. The proposed methodology can easily be implemented in image-centric databases enabling "real-time" image-based queries generating voxel-wise or region-wise statistical comparisons between subject subgroups stratified according to other, non-imaging variables. By appropriate parametrization of spatial distribution, the inverse approach will also be feasible and enable unsupervised biomarker discovery strategies seeking linkage between distinct lesion distribution patterns and yet unknown etiologic or pathogenic factors. The implementation of the proposed approach in large-scale MRI databases would enable both the automatic spatial analysis of newly acquired datasets as well as the efficient on-demand alignment of any pair or group of images.

References:

1. Mazziotta J, et al. A four-dimensional probabilistic atlas of the human brain. J Am Med Inform Assoc 2001; 8(5): 401-30.
2. Jenkinson M and Smith S. A global optimisation method for robust affine registration of brain images. Med Image Anal 2001; 5(2): 143-56.
3. Meier DS and Guttmann CR. Time-series analysis of MRI intensity patterns in multiple sclerosis. Neuroimage 2003; 20(2): 1193-209.
4. Wei X, et al. Quantitative analysis of MRI signal abnormalities of brain white matter with high reproducibility and accuracy. J Magn Reson Imaging 2002; 15(2): 203-9.
5. Charil A, et al. Statistical mapping analysis of lesion location and neurological disability in multiple sclerosis: application to 452 patient data sets. Neuroimage 2003; 19(3): 532-44.